# Deflection of an elliptically loaded vortex sheet by a flat plate

**JASON O. ARCHER**[1]†,

[1] Department of Mathematics and Statistics, University of New Mexico, Albuquerque, NM 87131, USA

(Received 19 April 2014)

We investigate the behavior of vortex flows in the presence of obstacles using numerical simulations. Specifically, we simulate the evolution of an elliptically loaded vortex sheet in the presence of a stationary flat plate in its path. The plate is represented by a number of point vortices whose strength is such that they cancel the normal fluid velocity on the plate. The sheet is approximated by a number of smoothed point vortices called vortex blobs. The resulting system of ordinary differential equations is solved using the 4th order Runge-Kutta method. In our simulations, we vary the initial distance $d$ from the vortex sheet to the plate, the angle $\phi$ of the plate relative to the sheet, and the numerical smoothing parameter $\delta$. We study the effects these parameters have on the vortex sheet evolution, including the positions of the vortex centers and the vortex sheet midpoint. We also compare with results derived from a simpler model using only two point vortices instead of a whole sheet. Our main conclusions regard the effect of the distance $d$, which reduces the total distance traveled as it is increased, and the angle $\phi$, which significantly affects the vortex trajectory after it encounters the plate.

## 1. Introduction

As planes fly through air, vorticity is shed from their wings and is left behind in the wake of the plane. The shed vorticity concentrates in a layer, which rolls up into two trailing vortices that travel downward. The air forced down by these vortices is often referred to as downwash, with a downwards force of opposite sign and proportional in magnitude to the upwards lift force acting on the plane. The strong force caused by the trailing vortices of large planes can cause smaller airplanes flying behind them to crash. Preventing such effects on following airplanes is the primary reason airports limit times between takeoffs and landings. However, crashes still occur sometimes when an aircraft flies into another aircraft's path too soon. One example is the Piper Navajo crash in Richmond, British Columbia in July 9, 2009 [http://www.cbc.ca/news/canada/british-columbia/story/2009/07/10/richmond-plane-crash.html], which was flying behind an Air Canada Airbus 321. Therefore much effort has been made to find mechanisms that reduce the strength of the separated vorticity. For example, Rennich and Lele (1999) and Leonard (1980) recommend mitigating trailing vortices' effects by redesigning the airfoils to create opposite signed vorticity that speeds up the viscous decay of the lead vorticity. A review of the formation, motion, and persistence of trailing vortices relevant to air travel is given by Spalart (1998).

In this paper we study the interaction of the trailing vorticity with obstacles in its path. Following Baker (1979) and Krasny (1987), we model the 3-dimensional shed vorticity layer by a planar 2-dimensional vortex sheet. The vortex sheet model consists of replacing

† Email address for correspondence: jason.o.archer@gmail.com

the vortex layer of finite thickness by a surface of zero thickness. The fluid is assumed to be inviscid, and is irrotational away from the surface. The velocity component tangential to the surface is discontinuous across it. The velocity jump across the sheet is the vortex sheet strength. Our initial conditions consist of the elliptically loaded vortex sheet which induces flow past a flat plate.

We compute the evolution of the vortex sheet in the presence of a flat plate in its path. The plate is, in turn, modeled as a sheet, whose strength is such that the normal fluid velocity is zero on the plate wall. The free vortex sheet rolls up into a pair of vortices approximating the trailing vortices. We find that the trajectory of this vortex pair is deflected by the flat plate and study the amount of deflection as a function of the initial distance between the sheet and the plate, and the angle of the plate relative to the initial sheet. We also compare the vortex sheet results with those using a simple model in which the trailing vortex is approximated by two point vortices.

Computing vortex sheet motion has a long history dating back to the numerical works of Higdon and Pozrikidis (1985), Baker (1980), Saffman and Baker (1979), and Fink and Soh (1978). Also see the review given by Sarpkaya (1989). These simulations are based on approximating the sheet by point vortices and evolving these points using an approximate set of governing ordinary differential equations. However, the early results did not converge under mesh refinement. It was not until the work of Moore (1979) and Krasny (1986ab) that some insight was gained as to the causes for the irregular point vortex motion. Moore considered a periodic vortex sheet with analytic initial data, and showed that, because of the Kelvin-Helmholtz instability of the sheet, the sheet does not remain analytic at all times but develops a singularity in finite time. At that time the vortex sheet strength and the sheet curvature become unbounded at a point on the sheet. Krasny (1986a) showed that before that time, high wavenumber oscillations introduced numerically due to roundoff error grow exponentially fast due to the Kelvin-Helmholtz instability of the sheet, leading to noisy results. He introduced a Fourier filter, in which all modes at the level of machine precision are truncated at each timestep in the simulation. This filter prevents the growth of artificially introduced large wavenumbers. Numerical simulations by Krasny (1986a) and Shelley (1992), and analytical work of Caflish, Ercolani, Hou and Landis (1993) show that before the time of singularity formation, the results computed with the Krasny filter converge as the spatial and time discretization is refined, and the filter level decreased. However, Krasny also showed that past the time of singularity formation, the filtered computations do not converge. The approach he took to compute the motion past this time is to regularize the vortex sheet motion by introducing a smoothing parameter into the governing equation. In effect, the sheet is approximated by a finite number of regularized point vortices referred to as vortex blobs [Chorin and Bernard (1973), Anderson (1986), and Krasny (1986b)]. The regularized periodic sheet studied by Moore rolls up into a sequence of vortices, mimicking what is observed in laboratory experiments. Comparison of vortex blob simulations with viscous simulation [Tryggvason et al. (1991), Sheng et al. (2012)] and with laboratory experiment [Nitsche and Krasny (1994)] shows that the regularized vortex sheet simulations approximate the viscous flow well.

Here, we simulate the free vortex sheet modeling the wake of a plane using the regularized vortex blob approximation. The free sheet rolls up at its edges into a double-spiral forming two counter-rotating vortices. These vortices travel downstream in direction of the plate, and move around the plate. We study the effect of the regularization parameter, the distance between the initial sheet and the plate, and the angle of inclination of the plate. We observed the following trends. As we reduce the vortex blob parameter, the vortex spiral develops more turns and travels slightly faster. However, the trajectories of

the vortex centers, and of the two-point-vortex approximation seem unchanged. On the other hand, modifying the distance between the initial vortex sheet and the plate changes the total distance travelled by the free sheet. If the sheet starts out close to the flat plate, it travels noticeably further than in the absence of a plate. For larger initial distances between the plate and the sheet, the sheet travels less far. Changing the inclination of the plate deflects the trajectory of the plate. Here, interestingly, for small values of $\phi$ the trajectory is deflected in the direction of the orientation of the plate, leaving at a small angle from the direction of approach, normal to the plate. However, for large values, the vortex trajectory is deflected in the direction opposite to the orientation of the plate, leaving in the direction parallel to the plate. In all cases studied, the vortex pair approximation of the sheet behaved qualitatively similar to the vortex sheet trajectory. Small quantitative differences between the sheet and the point vortex pair are observed in the case of flow plast an inclined plate, with small changes in the angle of deflection of the vortex motion.

The paper is organized as follows. Section 2 describes the problem considered here. In Section 3, we present the governing equations, the discrete approximation by a system of ordinary differential equations, and the numerical method to solve them. Section 4 presents the numerical results. The results are summarized in Section 5.

## 2. Problem Description

### 2.1. *Shear layer separation behind airfoil*

When fluid moves past walls, fluid viscosity causes particles to stick to the wall. This creates large velocity gradients and thereby introduces nonzero rotation into the flow. The fluid rotation is measured by the vorticity. This is easiest to see using a simple example of planar two-dimensional flow.

First, we introduce the variables describing the fluid flow. In Cartesion coordinates $\boldsymbol{x} = (x, y, z)$, the velocity field is given by

$$\boldsymbol{u}(\boldsymbol{x}, t) = (u(\boldsymbol{x}, t), v(\boldsymbol{x}, t), w(\boldsymbol{x}, t)) \tag{2.1}$$

where $u, v, w$ are the velocity components in the $x$-, $y$-, and $z$-direction respectively. The fluid rotation is measured by the vorticity

$$\nabla \times \boldsymbol{u} = (\frac{\partial w}{\partial y} - \frac{\partial v}{\partial z}, \frac{\partial u}{\partial z} - \frac{\partial w}{\partial x}, \frac{\partial v}{\partial x} - \frac{\partial u}{\partial y}) \ . \tag{2.2}$$

Specifically, at a point in the flow domain at which the vorticity vector is nonzero, the fluid rotates in a plane normal to the vorticity with angular velocity equal to half of the vorticity magnitude. Planar two-dimensional flow refers to the case when there is no velocity component in the $z$-direction, and no changes in the $z$-direction, $w = 0$ and $\partial/\partial z = 0$. In that case the velocity and vorticity reduce to

$$\boldsymbol{u}(\boldsymbol{x}, t) = (u(x, y, t), v(x, y, t), 0) \ , \tag{2.3a}$$

$$\nabla \times \boldsymbol{u} = (0, 0, \omega \ ) \tag{2.3b}$$

where $\omega = \frac{\partial v}{\partial x} - \frac{\partial u}{\partial y}$ is the scalar vorticity. That is, the vorticity is a vector pointing in the z-direction. If $\omega > 0$, fluid rotates in the $xy$-plane, normal to the vorticity, in the counterclockwise direction. If $\omega < 0$, the rotation is clockwise. For planar flows, we will not list the third zero component of the velocity field.

Now consider the simple example of planar flow parallel to a flat wall at $y = 0$. In the absence of viscosity, the uniformly parallel flow $(U, 0)$, illustrated in figure 1(a), solves

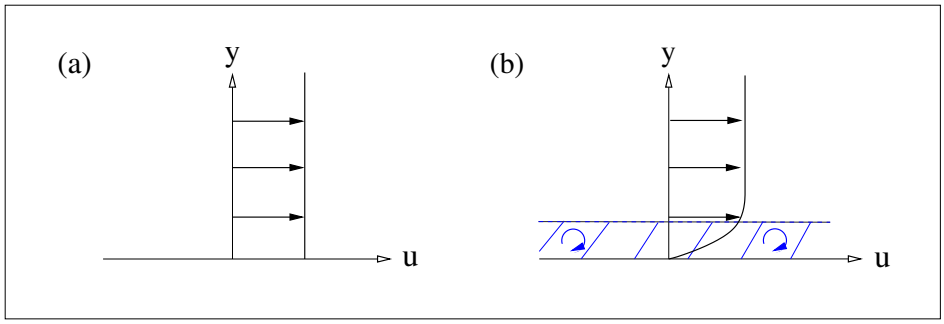


Figure 1: Velocity profiles in parallel flow past a wall. (a) Inviscid flow. (b) Viscous flow with boundary layer of clockwise rotating vorticity (in blue).

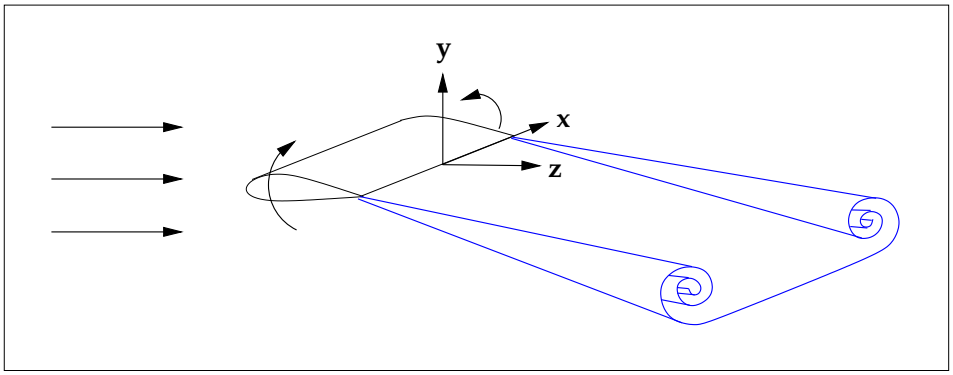


Figure 2: Sketch showing shear layer separation and rollup behind an airfoil in oncoming flow, that is parallel and uniform in the far field, with magnitude $U$.

the governing Euler Equations. On the other hand, in the presence of viscosity, the fluid velocity must vanish at the wall. Thus a transition region forms between the wall and the far field velocity in which the velocity decreases in magnitude from $U$ to zero; see the region indicated in blue in figure 1(b). Within this boundary layer the velocity gradients, in particular $\frac{\partial u}{\partial y}$ in this case, are large, leading to large negative vorticity. The vorticity is carried downstream with the fluid velocity and can separate at corners or regions of large curvature. The flow within a separated layer of vorticity with large velocity gradients is referred to as a shear flow.

Figure 2 is an idealized schematic of the three-dimensional generation and separation of vorticity in flow past an airfoil. The vorticity, shown in blue, is generated around the wing and separates as a shear layer that rolls up into a spiral along each of the wing tip flat edges. The vorticity concentrates within the spirals, and forms the trailing vortices often observed behind flying planes, also referred to as contrails. The fluid velocity is large within the vortices, which, according to Bernoulli's law, leads to small air pressure in this region. As a result, water vapor in the air condensates forming a mini-cloud, which is what makes the contrails behind the plane visible. The two trailing vortices induce a downward motion on each other, which is felt as downwash when the plane is near the ground.

For reference below, we let $\boldsymbol{x} = (x, y, z)$ denote the coordinates of a point in the Cartesian coordinate system illustrated in figure 2, with the $xy$-plane parallel to the span of the airfoil, the $z$-axis normal to it, with the origin at the center of the trailing

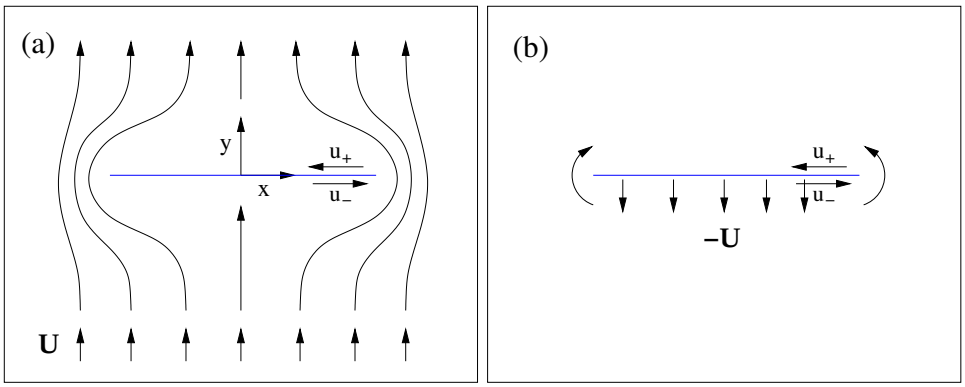


Figure 3: Sketch showing the initial vortex sheet, in blue, mimicking the shear layer behind the plane at $z = 0$. The sheet induces flow past it, from below to above, shown in black, with no fluid flowing through the sheet. (a) Reference frame fixed on the sheet. (b) Reference frame fixed at infinity.

edge of the wing. We consider a reference frame in which the airfoil is stationary, so that the oncoming fluid flow is in direction of the $z$-axis.

### 2.2. *Free vortex sheet model for separated shear layer*

Following Krasny (1987), we now model the separated shear layer by an elliptically loaded planar vortex sheet. The vortex sheet approximates the shear layer by a surface across which the tangential velocity is discontinuous. The fluid is assumed to be inviscid, and the vorticity is zero away from the sheet. The initial sheet is chosen so as to approximate the idealized shear layer behind the airfoil, illustrated in figure 2 downstream of the wing. That is, it is chosen to be flat with velocity jump across the sheet prescribed to be such that it induces flow past the sheet but with no fluid flowing through the sheet. The resulting vorticity distribution yields the sheet referred to as "elliptically loaded". The flow moves from the bottom to the top of the sheet, mimicking the flow from bottom to top around the sides of the airfoil. This initial sheet and the induced flow is sketched in figure 3. In figure 3(a), the flow is shown in a reference frame in which the velocity at the sheet vanishes, and the flow is upward and uniform with constant value $\mathbf{U}$ at infinity. In our computations we use the reference frame shown in 3(b), in which the velocity at infinity vanishes, and the initial velocity is downward and uniform on the plate. It is obtained from the flow in 3(a) by adding a potential flow $-\mathbf{U}$ to it.

The sheet is allowed to move freely under its self-induced motion. As will be seen, as time increases the sheet rolls up at its edges as it moves downward, corresponding to a crossection of the idealized shear layer in figure 2 at $z > 0$.

The vortex sheet is defined by its position

$$\boldsymbol{x}(\alpha, t) = (x(\alpha, t), y(\alpha, t)) \ , \tag{2.4}$$

and by the distribution of vorticity along the sheet. The vorticity distribution is described by the circulation function $\Gamma(\alpha)$, where

$$\Gamma(\alpha) = \int_{\partial D} \boldsymbol{u} \cdot \boldsymbol{T} ds = \int_D \nabla \times \boldsymbol{u} \cdot \boldsymbol{n} dA = \int_D (0, 0, \omega) \cdot (0, 0, 1) dA = \int_D \omega dA \ , \tag{2.5}$$

and $\partial D$ is a curve enclosing the sheet between $x = 0$ and $x = x(\alpha, t)$. As applied in equation (2.5), Stokes theorem shows that $\Gamma$ measures the integral amount of vorticity

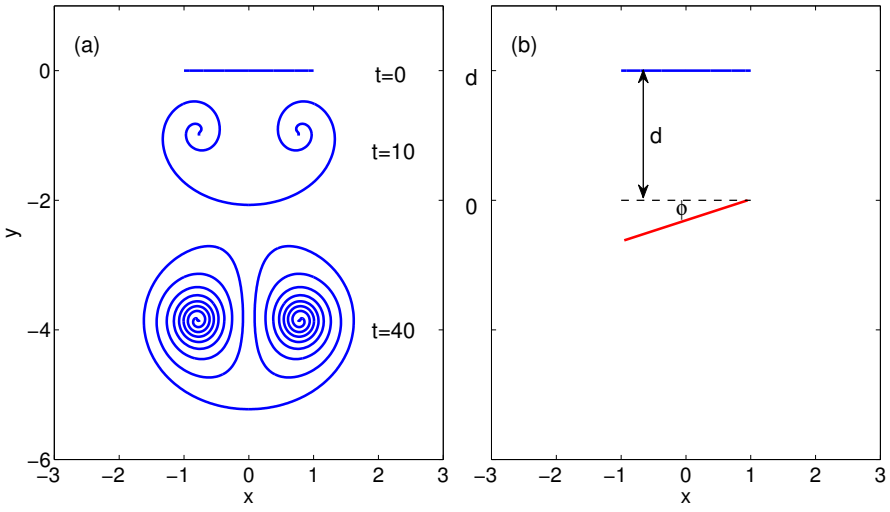


Figure 4: (a) Evolution of the initially flat vortex sheet (blue) under its self-induced velocity, in the absence of a plate, at the indicated times. (b) Position of the plate (red) relative to the initial vortex sheet, illustrating the vertical distance $d$, and plate angle $\phi$.

in this portion of the sheet. One can show that $\Gamma$ is related to the jump in the tangential velocity component across the sheet by

$$\frac{d\Gamma}{ds} = -(u_+ - u_-) = \sigma(s,t) \tag{2.6}$$

where $s$ is arclength, and $u_\pm$ are the limiting tangential velocities from above and below the plate respectively. The quantity $\sigma(s,t)$ is referred to as the vortex sheet strength. If the points $x(\alpha,t), y(\alpha,t)$ move with the average of the velocities above and below the sheet, then $\Gamma(\alpha)$ is independent of time. However, the sheet strength $\sigma$ at a given point $\alpha$ does depend on time.

The elliptically loaded initally flat sheet illustrated in figure 3, non-dimensionalized to have unit half-length and unit circulation around half the sheet, is given by

$$x(\alpha,0) = \cos(\alpha)\ , \tag{2.7a}$$
$$y(\alpha,0) = 0\ , \tag{2.7b}$$
$$\Gamma(\alpha) = \sin(\alpha)\ , \tag{2.7c}$$

with $\alpha \in [0,\pi]$. The corresponding non-dimensionalization initial downward sheet velocity is $-\mathbf{U} = (0,-1/4)$. Notice that this initial sheet has singularities near the endpoints $x = \pm 1$. Since

$$\Gamma(s) = \Gamma(x) = \sqrt{1-x^2}\ , \tag{2.8}$$

it follows that the velocity jump,

$$\frac{d\Gamma}{ds} = \frac{d\Gamma}{dx} = \frac{d\Gamma}{d\alpha}\cdot\frac{d\alpha}{dx} = -\frac{x}{\sqrt{(1-x^2)}}\ , \tag{2.9}$$

becomes unbounded as $x$ approaches 1.

### 2.3. *Bound Vortex Sheet Model for Plate*

We consider the evolution of the initially flat vortex sheet under its self-induced velocity. In the absence of an obstacle in its path, Krasny (1987) showed that the sheet rolls up at

its edges as it moves downward, as shown in figure 4(a). In this paper, we consider how the evolution is altered if a flat, rigid plate is positioned in its path, as shown in figure 4(b). The plate is positioned at distance $d$ below the initial vortex sheet, and is inclined at an angle $\phi$ from the horizontal. In our inviscid model, the plate modifies the total fluid velocity by adding a component to it that ensures that no flow passes through it. We are interested in the effect of the vertical distance $d$ between the plate and the sheet, and of the inclination angle $\phi$ on the evolution of the free vortex sheet.

Herein, we change reference frame and place the initial free sheet at $y = d$, with the plate at $y = 0$ as shown in figure 4. The position of the plate is described by

$$\boldsymbol{x}_p(\beta) = (\cos\beta\cos\phi, \cos\beta\sin\phi - |\sin\phi|) \ , \quad \beta = [0, \pi] \ . \tag{2.10}$$

The plate is modelled by a fixed vortex sheet in its place whose strength $\sigma_p$ is such that the normal fluid velocity on the plate vanishes. As we will see, this results in a linear system that determines the discretized vortex strength on the plate.

## 3. Governing Equations

### 3.1. *Euler Equations*

Vortex sheet flow is governed by the Euler equations for inviscid, incompressible flow. These are a set of partial differential equations obtained from conservation of mass and momentum, under the assumption that there are no friction forces parallel to solid walls immersed in the fluid, and no viscous diffusion. The incompressible Euler equations for fluid in a domain $D$ bounded by solid walls are given by

$$\frac{D\rho}{Dt} = 0 \quad \text{in} D \ , \tag{3.1a}$$

$$\rho\frac{D\boldsymbol{u}}{Dt} = -\nabla p \quad \text{in} D \ , \tag{3.1b}$$

$$\nabla\cdot\boldsymbol{u} = \boldsymbol{0} \quad \text{in} D \ , \tag{3.1c}$$

$$\boldsymbol{u}\cdot\boldsymbol{n} = \boldsymbol{U}_{wall}\cdot\boldsymbol{n} \quad \text{on}\, \partial D \ , \tag{3.1d}$$

where $\rho = \rho(\boldsymbol{x}, t)$ is the fluid density, $\boldsymbol{u} = \boldsymbol{u}(\boldsymbol{x}, t) = (u(\boldsymbol{x}, t), v(\boldsymbol{x}, t))$ is the fluid velocity, $p = p(\boldsymbol{x}, t)$ is the fluid pressure, and $\boldsymbol{U}_{wall}$ is the wall/boundary velocity (which is equal to 0 if the wall is stationary). Throughout, $\boldsymbol{x} = (x, y)$. The gradient operator is $\nabla = (\partial/\partial x, \partial/\partial y)$, and the material derivative is $\frac{D}{Dt} = \frac{\partial}{\partial t} + \boldsymbol{u}\cdot\nabla = \frac{\partial}{\partial t} + u\frac{\partial}{\partial x} + v\frac{\partial}{\partial y}$. The boundary condition 3.1(d) states that the fluid velocity is parallel to the walls, but the parallel component is not necessarily zero.

For homogeneous incompressible planar flow, for which $\rho(\boldsymbol{x}, t) = \rho_0$ is constant throughout the fluid, the Euler equations imply that the scalar vorticity is constant on particles moving with the flow,

$$\frac{D\omega}{Dt} = 0 \ . \tag{3.2}$$

Furthermore, we know from vector calculus that for incompressible planar flow there exists a streamfunction $\psi(x, y, t)$ whose level curves are streamlines of the flow. It is determined uniquely, up to a constant, by the fluid velocity from

$$\frac{\partial\psi}{\partial x} = -v \ , \quad \frac{\partial\psi}{\partial y} = u \ . \tag{3.3}$$

Conventionally, the constant is set to be such that $\psi = 0$ on the walls. Thus, the stream-

function is alternatively determined by the vorticity from

$$\nabla^2\psi = -v_x + u_y = -\omega \ \text{ in } D\ , \quad \psi = 0 \text{ on } \partial D \tag{3.4}$$

In infinite domain $\mathbb{R}^2$, with vanishing velocity at infinity, the solution to the Poisson equation (3.4) is known to be

$$\psi(\boldsymbol{x},t) = -\frac{1}{2\pi}\int \omega(\boldsymbol{x}',t)\ln|\boldsymbol{x}-\boldsymbol{x}'|d\boldsymbol{x}'\ . \tag{3.5}$$

Given the vorticity in the fluid, the velocity is recovered from equations (3.3). In the presence of solid bodies in the flow, the fluid velocity is given by

$$\boldsymbol{u}(\boldsymbol{x},t) = \frac{1}{2\pi}\int \frac{(-(y-y'),x-x')}{(x-x')^2+(y-y')^2}\omega(\boldsymbol{x}',t)d\boldsymbol{x}' + \nabla\Phi(\boldsymbol{x},t) \tag{3.6}$$

where $\nabla\Phi$ is the potential flow that ensures that the total velocity is parallel to the solid walls on the boundary of the domain.

Given the fluid vorticity, the fluid velocity is thus recovered from (3.6). The velocity in turn determines the vorticity evolution through equation (3.2). This is the main idea of the vortex method used in this paper, described in §4. The next section describes the specific form of (3.6) for the vortex sheet flow past a plate.

### 3.2. *Vortex sheet flow past a plate*

For a vortex sheet, the vorticity is a delta function on the sheet and the integral in equation (3.6) reduces to a line integral over the sheet. For circulation distribution $\Gamma(\alpha)$, the resulting velocity induced by the sheet vorticity at a point $\boldsymbol{x}(\alpha,t) = (x(\alpha,t),y(\alpha,t))$ on the sheet is

$$\boldsymbol{u}(\boldsymbol{x}(\alpha,t),t) = \frac{1}{2\pi}\int_0^\pi \frac{(-(y-y'),x-x')}{(x-x')^2+(y-y')^2+\delta^2}\ \frac{d\Gamma}{d\alpha}(\alpha')\ d\alpha' + \nabla\Phi(\boldsymbol{x}(\alpha,t),t)\ , \tag{3.7}$$

where $(x,y) = (x(\alpha,t),y(\alpha,t))$ and $(x',y') = (x(\alpha',t),y(\alpha',t))$. Here, the parameter $\delta$ is introduced in the denominator to regularize the motion, following Krasny (1986b). This is necessary since otherwise the equations yield irregular particle motion.

In our case, $\boldsymbol{x}(\alpha,t)$ and $\Gamma(\alpha)$ represent the free vortex sheet simulating the separated shear layer behind the plane, initially given by equation (2.7$c$), and $\nabla\Phi(\boldsymbol{x}(\alpha,t))$ is the potential flow that vanishes at infinity and cancels the normal fluid velocity on the plate. It is induced by a second vortex sheet with position $\boldsymbol{x}_p(\beta)$ bound to the plate, whose vorticity distribution given by the strength $\sigma_p = d\Gamma_p/ds$ is such that the normal fluid velocity on the plate is cancelled. The resulting potential flow induced by the bound sheet at a point $\boldsymbol{x}$ away from the plate is given by

$$\nabla\Phi(\boldsymbol{x},t)) = \frac{1}{2\pi}\int_0^\pi \frac{(-(y-y_p'),x-x')}{(x-x_p')^2+(y-y_p')^2}\ \frac{d\Gamma_p}{d\beta}(\beta',t)\ d\beta' \tag{3.8}$$

where $(x_p',y_p') = (x_p(\beta'),y_p(\beta'))$.

The position $\boldsymbol{x}_p(\beta)$ is given by equation (2.10). The circulation $\Gamma_p(\beta,t)$ is determined from the equation

$$\boldsymbol{u}(\boldsymbol{x}_p(\beta),t)\cdot\boldsymbol{n}_p = 0 \quad \text{where} \quad \boldsymbol{n}_p = (-\sin\phi,\cos\phi)\ , \tag{3.9}$$

and $\phi$ is the plate angle shown in figure 4b. Here, $\boldsymbol{u}(\boldsymbol{x}_p(\beta),t)$ is the total velocity given by equations (3.7,3.8) at a point on the plate.

Note that the line integral in (3.8) has not been regularized by $\delta$. This is necessary for the following reason. As will be seen in the next section, upon discretizing, equation (3.9)

determines a linear system for the discrete vortex sheet strength. This system is solved at each time step to determine $\Gamma_p(\beta,t)$. The system is invertible only if the integral over the bound sheet in equation (3.8) is not regularized.

As a result, in order to evaluate the velocity at points on the plate, the integral in (3.8) must be considered in the principal value sense. The Plemelj equations (e.g., see Muskhelishvili 1953) show that the principal value integral equals the average of the limiting velocities above and below the sheet. At a point away from the plate, the integral in (3.8) is proper and no principal value needs to be taken.

In sumary, the evolution of the free vortex sheet $\boldsymbol{x}(\alpha,t)$ in the presence of the plate is given by

$$\begin{aligned}\frac{d\boldsymbol{x}}{dt}(\alpha,t) &= \frac{1}{2\pi}\int_0^\pi \frac{-(y-y'),(x-x')}{(x-x')^2+(y-y')^2+\delta^2}\frac{d\Gamma}{d\alpha}(\alpha')\,d\alpha' \\ &\quad + \frac{1}{2\pi}\int_0^\pi \frac{-(y-y'_p),(x-x'_p)}{(x-x'_p)^2+(y-y'_p)^2}\frac{d\Gamma_p}{d\beta}(\beta')\,d\beta'\end{aligned} \tag{3.10}$$

with initial conditions $\boldsymbol{x}(\alpha,0)=(x(\alpha,0),y(\alpha,0))$ and $\Gamma(\alpha)$ given by equation (2.7$c$). Notice that the free sheet $\boldsymbol{x}(\alpha,t)$ is always at some distance from the plate, so the second integral in (3.10) is not of principal value type. The solution of this system of two ordinary differential equations is the one we are interested in here.

## 4. Numerical Method

### 4.1. *Discretization*

The free vortex sheet is approximated by a set of $N+1$ regularized point vortices with position and circulation $\boldsymbol{x}_j(t)$ and $\Delta\Gamma_j$, $j=0,\ldots,N$. Their initial position is given by $\boldsymbol{x}_j(0)=\boldsymbol{x}(\alpha_j,0), \alpha_j=j\pi/N$. Their circulation is given by

$$\Delta\Gamma_j=\frac{d\Gamma}{d\alpha}(\alpha_j)\Delta\alpha_j$$

where $\Delta\alpha_j=(\alpha_{j+1}-\alpha_{j-1})/2$, $j=1,\ldots,N-1$, and $\Delta\alpha_0=\alpha_1-\alpha_0$ $\Delta\alpha_N=\alpha_N-\alpha_{N-1}$ These are the trapezoid rule weights of the discretization of (3.10) given below.

The bound vortex sheet is approximated by a set of $N_p+1$ point vortices with position and circulation $\boldsymbol{x}_{p,j}=\boldsymbol{x}_p(\beta_j)$, $\beta_j=j\pi/N$ and $\Delta\Gamma_{p,j}$, $j=0,\ldots,N_p$. These circulations are determined at each time step as explained shortly.

With this discretization, the regularized point vortices representing the free vortex sheet are evolved using an approximation of equations (3.10), obtained using the trapezoid rule,

$$\begin{aligned}\frac{d\boldsymbol{x}_j}{dt} &= \frac{1}{2\pi}\sum_{k=0}^{N}\frac{-(y_j-y_k),(x_j-x_k)}{(x_j-x_k)^2+(y_j-y_k)^2+\delta^2}\Delta\Gamma_k \\ &\quad + \frac{1}{2\pi}\sum_{k=0}^{N_p}\frac{-(y_j-y_{p,k}),(x_j-x_{p,k})}{(x_j-x_{p,k})^2+(y_j-y_{p,k})^2}\Delta\Gamma_{p,k}\ ,\end{aligned} \tag{4.1}$$

$j=0,\ldots,N$.

The plate circulations $\Delta\Gamma_{p,k}$ are obtained at each timestep by enforcing the discretized version of equation (3.9) at the $N_p$ midpoints on the plate,

$$\boldsymbol{x}^m_{p,j}=\boldsymbol{x}_p(\beta^m_j)\ ,\quad \beta^m_j=(\beta_j-\beta_{j-1})/2\ ,\quad j=1,\ldots,N_p\ . \tag{4.2}$$

The system of discretized equations $\boldsymbol{u}(\boldsymbol{x}^m_{p,j})\cdot\boldsymbol{n}_p=0$ is given by the following $N_p$ linear

equations in the $N_p + 1$ unknowns $\Delta\Gamma_{p,j}$

$$\begin{aligned} \sum_{k=0}^{N_p} \frac{\sin\phi(y^m_{p,j} - y_{p,k}) + \cos\phi(x^m_{p,j} - x_{p,k})}{(x^m_{p,j} - x_{p,k})^2 + (y^m_{p,j} - y_{p,k})^2} \Delta\Gamma_{p,k} \ . \\ = \quad -\sum_{k=0}^{N} \frac{\sin\phi(y^m_{p,j} - y_k) + \cos\phi(x^m_{p,j} - x_k)}{(x^m_{p,j} - x_k)^2 + (y^m_{p,j} - y_k)^2 + \delta^2} \Delta\Gamma_k \ . \end{aligned} \tag{4.3}$$

In order to uniquely solve for the $N_p+1$ unknowns, this system is augmented by enforcing that the total circulation in the flow be zero,

$$\sum_{k=0}^{N_p} \Delta\Gamma_{p,k} = 0 \ . \tag{4.4}$$

The linear system determining the bound vortex sheet circulations can be written as

$$A \cdot \Delta\mathbf{\Gamma_p} = \mathbf{b} \ , \tag{4.5}$$

as follows,

$$\begin{pmatrix} \frac{\sin\phi(y^m_{p,1}-y_{p,0})+\cos\phi(x^m_{p,1}-x_{p,0})}{(x^m_{p,1}-x_{p,0})^2+(y^m_{p,1}-y_{p,0})^2} & \cdots & \frac{\sin\phi(y^m_{p,1}-y_{p,N_p})+\cos\phi(x^m_{p,1}-x_{p,N_p})}{(x^m_{p,1}-x_{p,N_p})^2+(y^m_{p,1}-y_{p,N_p})^2} \\ \vdots & \ddots & \vdots \\ \frac{\sin\phi(y^m_{p,N_p}-y_{p,0})+\cos\phi(x^m_{p,N_p}-x_{p,0})}{(x^m_{p,N_p}-x_{p,0})^2+(y^m_{N_p}-y_{p,0})^2} & \cdots & \frac{\sin\phi(y^m_{p,N_p}-y_{p,N_p})+\cos\phi(x^m_{p,N_p}-x_{p,N_p})}{(x^m_{p,N_p}-x_{p,N_p})^2+(y^m_{N_p}-y_{p,N_p})^2} \\ 1 & \cdots & 1 \end{pmatrix} \begin{pmatrix} \Delta\Gamma_{p,0} \\ \vdots \\ \vdots \\ \Delta\Gamma_{p,N_p} \end{pmatrix}$$

$$= - \begin{pmatrix} \sum_{k=0}^{N} \frac{\sin\phi(y^m_{p,1}-y_k)+\cos\phi(x^m_{p,1}-x_k)}{(x^m_{p,1}-x_k)^2+(y^m_{1,p}-y_k)^2+\delta^2} \Delta\Gamma_k \\ \vdots \\ \sum_{k=0}^{N} \frac{\sin\phi(y^m_{p,N_p}-y_k)+\cos\phi(x^m_{p,N_p}-x_k)}{(x^m_{p,N_p}-x_k)^2+(y^m_{N_p,p}-y_k)^2+\delta^2} \Delta\Gamma_k \\ 0 \end{pmatrix} \tag{4.6}$$

Note that the matrix $A$ depends only on the bound vortex sheet position, which does not change in time. This system is solved at each timestep to obtain updated values of $\Delta\Gamma_{p,k}$.

### 4.2. *Time Steps*

The system of equations (4.1) is solved using the 4th-order Runge-Kutta method to step forward in time,

$$\begin{aligned} \left\{ \begin{array}{lcl} \boldsymbol{k}_1 &=& \Delta t \ \tilde{\boldsymbol{u}}(\tilde{\boldsymbol{x}}(t), t) \\ \boldsymbol{k}_2 &=& \Delta t \ \tilde{\boldsymbol{u}}(\tilde{\boldsymbol{x}}(t) + \boldsymbol{k}_1/2, t + \Delta t/2) \\ \boldsymbol{k}_3 &=& \Delta t \ \tilde{\boldsymbol{u}}(\tilde{\boldsymbol{x}}(t) + \boldsymbol{k}_2/2, t + \Delta t/2) \\ \boldsymbol{k}_4 &=& \Delta t \ \tilde{\boldsymbol{u}}(\tilde{\boldsymbol{x}}(t) + \boldsymbol{k}_3, t + \Delta t) \end{array} \right. \\ \tilde{\boldsymbol{x}}(t + \Delta t) = \tilde{\boldsymbol{x}}(t) + (\boldsymbol{k}_1 + 2\boldsymbol{k}_2 + 2\boldsymbol{k}_3 + \boldsymbol{k}_4)/6 \end{aligned} \tag{4.7}$$

where the tildes refer to the discrete approximations of $\boldsymbol{x}$ and $\boldsymbol{u}(\boldsymbol{x}, t)$, $\tilde{\boldsymbol{x}} = (\boldsymbol{x}_1(t), \ldots, \boldsymbol{x}_N(t))$, $\tilde{\boldsymbol{u}} = d\tilde{\boldsymbol{x}}/dt$. Note that the bound vortex sheet circulations $\Delta\Gamma_{p,k}$ are updated in each of the four Runge-Kutta stages.

In all of our simulations, we set our time step to be $\Delta t = 0.05$. If we set it larger than this, the sheet starts twisting and deforming in odd places. If we set it smaller than

this, there is no discernible improvement in simulation quality. In all our simulations, we approximated the bound vortex sheet by 600 points ($N_p = 599$). The free sheet is approximated initially by 1000 points ($N = 999$). As the free sheet evolves and stretches, new points are inserted to maintain resolution. This step is described next.

### 4.3. *Inserting new vortices in the free sheet*

As the free vortex sheet evolves it edges roll up into a spiral and the sheet is stretched. As a result, soon after the beginning of the motion, the initial number of 1000 regularized point vortices is insufficient to accurately represent the position of the vortex sheet. We therefore use a 3rd-order Lagrange interpolation formula to place new vortices into the vortex sheet as time progresses, interpolating in the $\alpha$ variable. Under certain conditions, described below, we insert a point in the middle of four pre-existing sequential points, as follows. Suppose the four pre-existing points have position $\boldsymbol{x}_{k-2}, \boldsymbol{x}_{k-1}, \boldsymbol{x}_k, \boldsymbol{x}_{k+1}$ and correspond to parameters $\alpha_{k-2}, \alpha_{k-1}, \alpha_k, \alpha_{k+1}$. The new point is inserted between the second and third point of these four. It is assigned a corresponding parameter of

$$\alpha_{new} = (\alpha_{k-1} + \alpha_k)/2$$

and given position

$$\begin{aligned}
\boldsymbol{x}_{new} = \boldsymbol{x}_{k-2} & \tfrac{(\alpha_k-\alpha_{k-1})(\alpha_k-\alpha_{k+1})(\alpha_k-\alpha_{k+2})}{(\alpha_{k-2}-\alpha_{k-1})(\alpha_{k-2}-\alpha_{k+1})(\alpha_{k-2}-\alpha_{k+2})} \\
+\boldsymbol{x}_{k-1} & \tfrac{(\alpha_k-\alpha_{k-2})(\alpha_k-\alpha_{k+1})(\alpha_k-\alpha_{k+2})}{(\alpha_{k-1}-\alpha_{k-2})(\alpha_{k-1}-\alpha_{k+1})(\alpha_{k-1}-\alpha_{k+2})} \\
+\boldsymbol{x}_{k+1} & \tfrac{(\alpha_k-\alpha_{k-2})(\alpha_k-\alpha_{k-1})(\alpha_k-\alpha_{k+2})}{(\alpha_{k+1}-\alpha_{k-2})(\alpha_{k+1}-\alpha_{k-1})(\alpha_{k+1}-\alpha_{k+2})} \\
+\boldsymbol{x}_{k+2} & \tfrac{(\alpha_k-\alpha_{k-2})(\alpha_k-\alpha_{k-1})(\alpha_k-\alpha_{k+1})}{(\alpha_{k+2}-\alpha_{k-2})(\alpha_{k+2}-\alpha_{k-1})(\alpha_{k+2}-\alpha_{k+1})}
\end{aligned} \tag{4.8}$$

and circulation

$$\Delta\Gamma_{new} = \Gamma(\alpha_{new})(\alpha_k - \alpha_{k-1})/2 \ .$$

To correctly represent the trapezoid rule approximation of the integrals, the circulations of the neighbouring points to the new point need to be corrected to

$$\Delta\Gamma_{k-1} = \Gamma(\alpha_{k-1})(\alpha_{new} - \alpha_{k-2})/2$$

$$\Delta\Gamma_k = \Gamma(\alpha_k)(\alpha_{k+1} - \alpha_{new})/2$$

All points are then reindexed from $k = 1, N + 2$, and the value of $N$ is increased by 1.

We use this formula to insert new points under the following criteria:

(1) Points are not inserted in the innermost loop in each of the two spiral centers. As will be seen below, the innermost loop has an inflection point near the end of the sheet. Points are not inserted between this inflection point and the end of the sheet. The inflection point within each spiral is determined by finding the point at which the crossproduct of two vectors between consecutive points

$$(x_k - x_{k-1}, y_k - y_{k-1}, 0) \times (x_{k+1} - x_k, y_{k+1} - y_k, 0)$$

changes sign. This inflection point, $\boldsymbol{x}_I$, is a good approximation of the spiral center.

(2) Points are inserted on the outer spiral turns if the spacing between the points is too large. Here, we ensure that the total number of points around one turn of the spiral is no less than a prescribed minimum, in our case 60 points. We thus insert a point if the angle two consequtive points $\boldsymbol{x}_{k-1}$, $\boldsymbol{x}_k$ make with the spiral center $\boldsymbol{x}_I$ is bigger than

$\pi/30$. This angle is computed using the Law of Cosines

$$\begin{array}{rcl} A^2 & = & ||\boldsymbol{x}_{k-1} - \boldsymbol{x}_I||^2 \\ B^2 & = & ||\boldsymbol{x}_k - \boldsymbol{x}_I||^2 \\ C^2 & = & ||\boldsymbol{x}_k - \boldsymbol{x}_{k-1}||^2 \\ \cos\theta & = & \frac{A^2+B^2-C^2}{2AB}; \end{array} \tag{4.9}$$

Each of the two spirals is considered separately.

(3) Points are not inserted outside of the spiral roll-up, past points on the sheet at which the curvature changes sharply. Past those points, point insertion proved to be too inaccurate. Thus, in our simulations the spiral roll-up is resolved, but the vortex sheet in the far field is not fully resolved. This aspect of our computation could be improved, but we will leave this for future work. The point at which the curvature $\kappa$ changes too fast was determined by trial and error to be the first point at which $d\kappa/d\alpha \geq 100000$. Taking the variable $s$ to be arc length, we approximate the curvature

$$\kappa = \left| \frac{d^2\boldsymbol{x}}{ds^2} \right|$$

as follows, using formulas for finite-difference derivative approximations:

$$\begin{array}{rcl} \Delta s_1 & = & ||\boldsymbol{x}_k - \boldsymbol{x}_{k-1}|| \ , \quad \Delta x_1 = x_k - x_{k-1} \ , \quad \Delta y_1 = y_k - y_{k-1} \ , \\ \Delta s_2 & = & ||\boldsymbol{x}_{k+1} - \boldsymbol{x}_k|| \ , \quad \Delta x_2 = x_{k+1} - x_k \ , \quad \Delta y_2 = y_{k+1} - y_k \ , \\ \kappa_k & = & 2\dfrac{\sqrt{(\Delta s_1 \Delta x_2 - \Delta s_2 \Delta x_1)^2 + (\Delta s_1 \Delta y_2 - \Delta s_2 \Delta y_1)^2}}{\Delta s_1 \Delta s_2 (\Delta s_1 + \Delta s_2)} \end{array} \tag{4.10}$$

The rate of change of curvature at a point $\boldsymbol{x}_k$ is approximated by

$$\left.\frac{d\kappa}{d\alpha}\right|_k = \frac{\kappa_{k+1} - \kappa_{k-1}}{\alpha_{k+1} - \alpha_{k-1}} \ . \tag{4.11}$$

### 4.4. *Two Vortex Approximation of Shear Layer*

We compare results of the vortex sheet model with an even simpler model in which the vortex sheet is replaced at $t = 0$ by two point vortices with circulation and center of mass equal to each half of the vortex sheet,

$$\boldsymbol{x}_l = \frac{\sum_{k=0}^{N/2} \boldsymbol{x}_k \Delta\Gamma_k}{\sum_{k=0}^{N/2} \Delta\Gamma_k} \ , \quad \boldsymbol{x}_r = \frac{\sum_{k=N/2}^{N} \boldsymbol{x}_k \Delta\Gamma_k}{\sum_{k=N/2}^{N} \Delta\Gamma_k} \ , \quad \Gamma_l = 1 \ , \quad \Gamma_r = -1 \ . \tag{4.12}$$

These two points are evolved in the flow equation according to the point vortex equations

$$\frac{d\boldsymbol{x}_l}{dt} = \frac{1}{2\pi} \frac{-(y_l - y_r), (x_l - x_r)}{(x_l - x_r)^2 + (y_l - y_r)^2} \Gamma_r + \frac{1}{2\pi} \sum_{k=0}^{N_p} \frac{-(y_l - y_{p,k}), (x_l - x_{p,k})}{(x_l - x_{p,k})^2 + (y_l - y_{p,k})^2} \Delta\Gamma_{p,k} \ ,$$

$$\frac{d\boldsymbol{x}_r}{dt} = \frac{1}{2\pi} \frac{-(y_r - y_l), (x_r - x_l)}{(x_r - x_l)^2 + (y_r - y_l)^2} \Gamma_l + \frac{1}{2\pi} \sum_{k=0}^{N_p} \frac{-(y_r - y_{p,k}), (x_r - x_{p,k})}{(x_r - x_{p,k})^2 + (y_r - y_{p,k})^2} \Delta\Gamma_{p,k} \ .$$

## 5. Results

This section presents the evolution of the vortex sheet and the two-point-vortex approximation computed as described above.

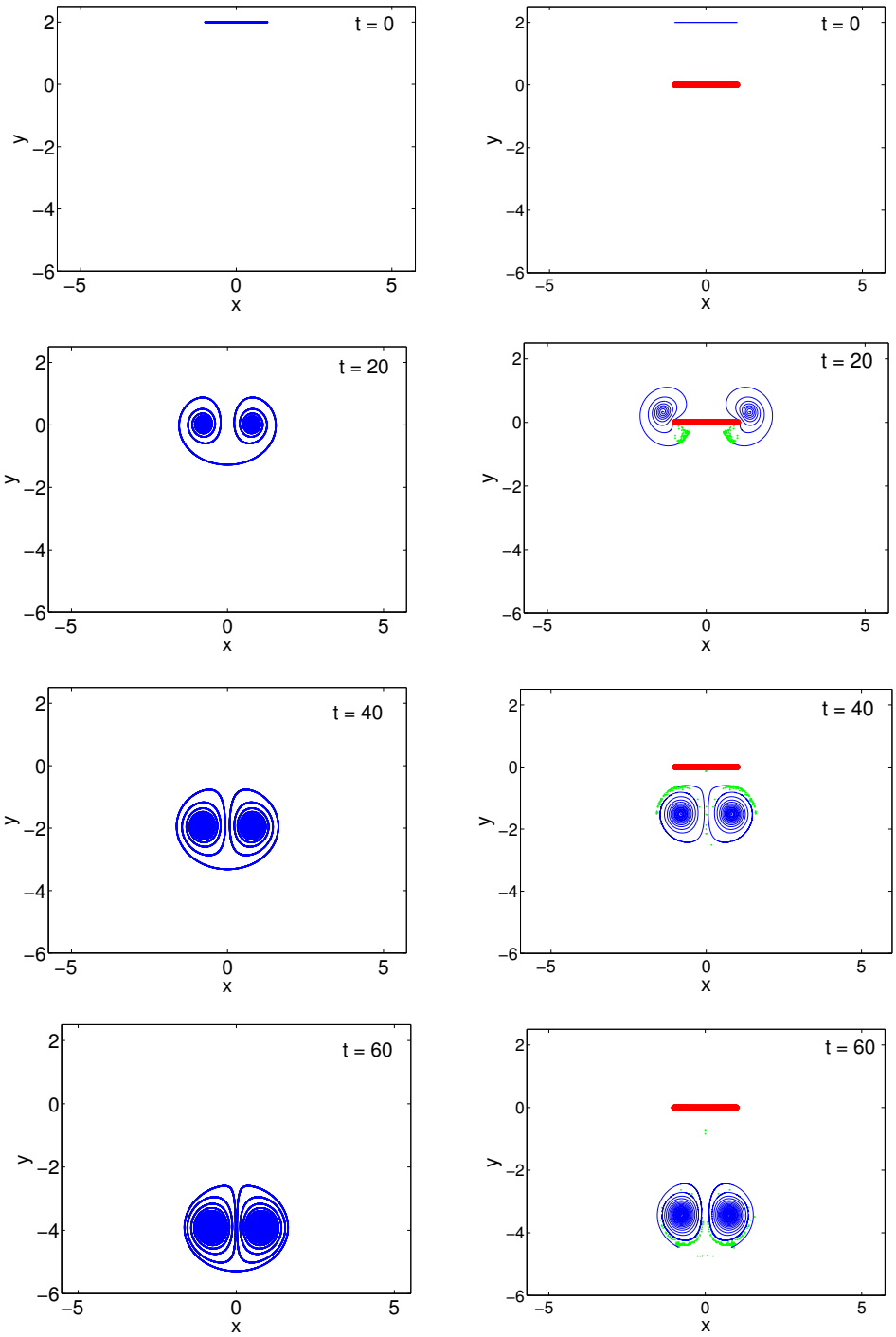


Figure 5: Comparison of vortex sheet evolution at the indicated times, in the absence of a plate (left column), with evolution in the presence of a plate at distance $d = 2$, with $\phi = 0$ (right column). Computations are performed with $\delta = 0.2$. .

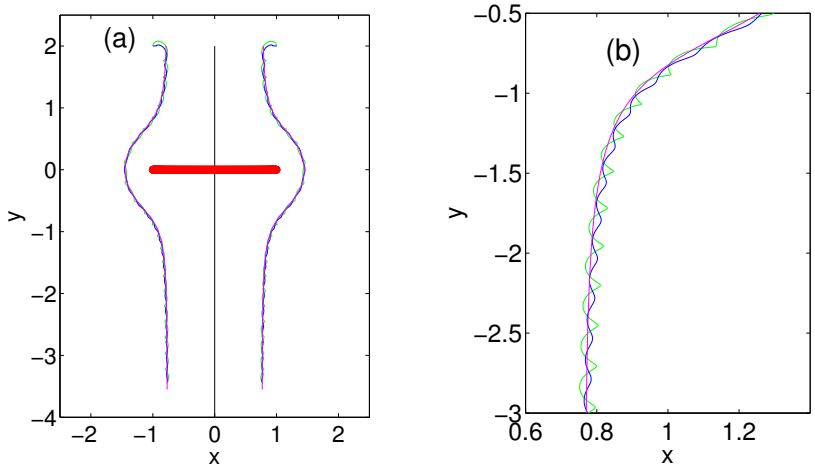


Figure 6: Trajectory of vortex core from $t = 0$ to $t = 60$, with $d = 2$, $\delta = 0.2$, $\phi = 0$. (a) Large scale showing vortex movement around plate. (b) Closeup showing the endpoint of the sheet (green), the position of the inflection point (blue), and the position of the point vortex pair approximation (purple).

### 5.1. *Vortex sheet evolution around plate, with* $d = 2, \phi = 0, \delta = 0.2$

Figure 5 compares the vortex sheet position at the indicated times, in the absence of a plate (left column) with the evolution in the presence of a plate at $d = 2$, with $\phi = 0$ (right column). In both cases, the computations are performed with $\delta = 0.2$.

The left column reproduces results in Krasny (1987). The sheet rolls up into a spiral around each of its edges as it travels downward. In the right column, a plate is positioned one sheet length below the initial sheet position. As the sheet rolls up and moves downward, it approaches the plate, and wraps around the plate around $t = 20$. Afterwards, the sheet continues its roll-up and downward motion. However, comparison with the left column shows that in the presence of the plate, the sheet has been slowed down. As a result it has not traveled as far at $t = 60$ as in the case of no plate. We note that in the right column, the sheet is shown in blue and green colors. The blue portion of the sheet is the one that is well-resolved by the point insertion algorithm. The green portion is the one that is underresolved due to regions of high curvature that form as the sheet approaches the plate. This green portion does not correspond exactly to the regions of high curvature exempted from interpolation by our criterion, but is edited for visual clarity. These high curvature regions make it difficult to resolve the flow better.

Figure 6 shows the trajectory of the two spiral vortex centers. For comparison, the position of the endpoints of the sheet (green) and the position of the inflection point near the endpoint (blue) are shown. The position of the two-point-vortex approximation of the vortex sheet is shown in purple. Figure 6(a) also plots the position of the midpoint of the sheet corresponding to parameter $\alpha = \pi/2$. Figure 6(a) shows that both spiral centers remain symmetric about the middle line. The centerpoint on the discretized vortex sheet travels straight downward after closely moving around the plate. The spiral centers move down and around the plate. The closeup in figure 6(b) shows that the three trajectories, approximating the spiral centers, follow each other closely. The endpoints and the inflection point oscillate slightly as they travel downstream, while the path of the two-point-vortex approximation is non-oscillatory. The two-point-vortex approximation

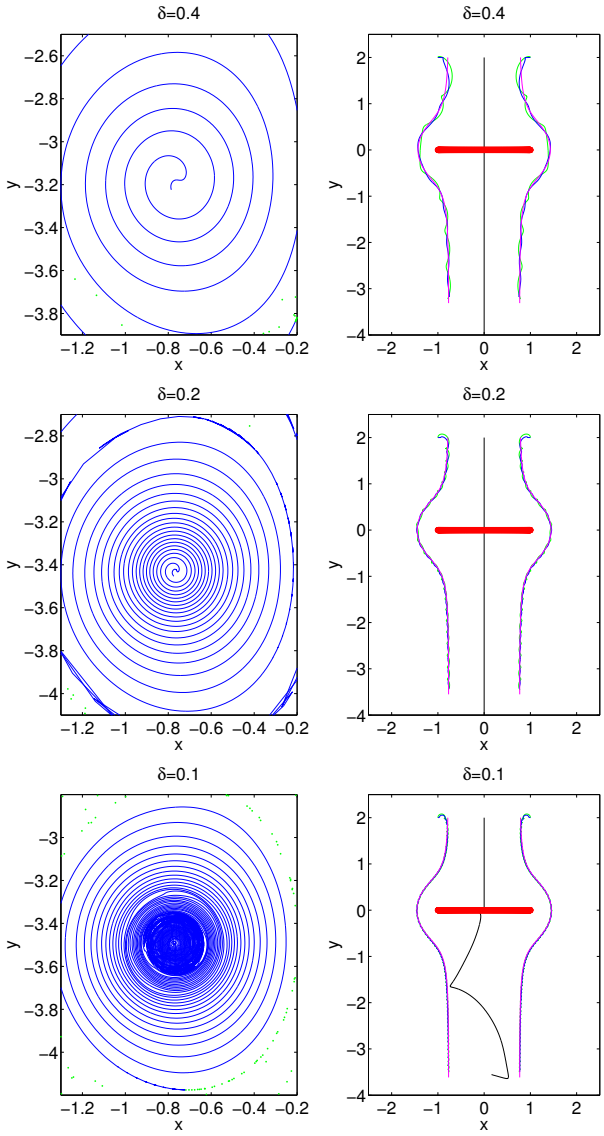


Figure 7: Solution for $\delta = 0.4, 0.2, 0.1$, as indicated, with $d = 2, \phi = 0$. Closeup of vortex sheet at $t = 60$ (left), and core trajectories (right).

travels slightly farther than the vortex sheet, but otherwise it models the vortex sheet trajectory remarkably well. The following sections discuss the dependence of the solution on the three parameters $\delta$, $d$, and $\phi$.

### 5.2. *Dependence on* $\delta$

Figure 7 shows the dependence of the solution on $\delta$, by comparing results with $\delta = 0.4, 0.2$ and 0.1. The left column shows a closeup of the left spiral center at the final time $t = 60$. As $\delta$ decreases, the number of spiral turns increases significantly. With the smallest value of $\delta = 0.1$, the number of spiral turns is so large we could not fully resolve it with our available computing time, which is in part the reason for the irregularities that can

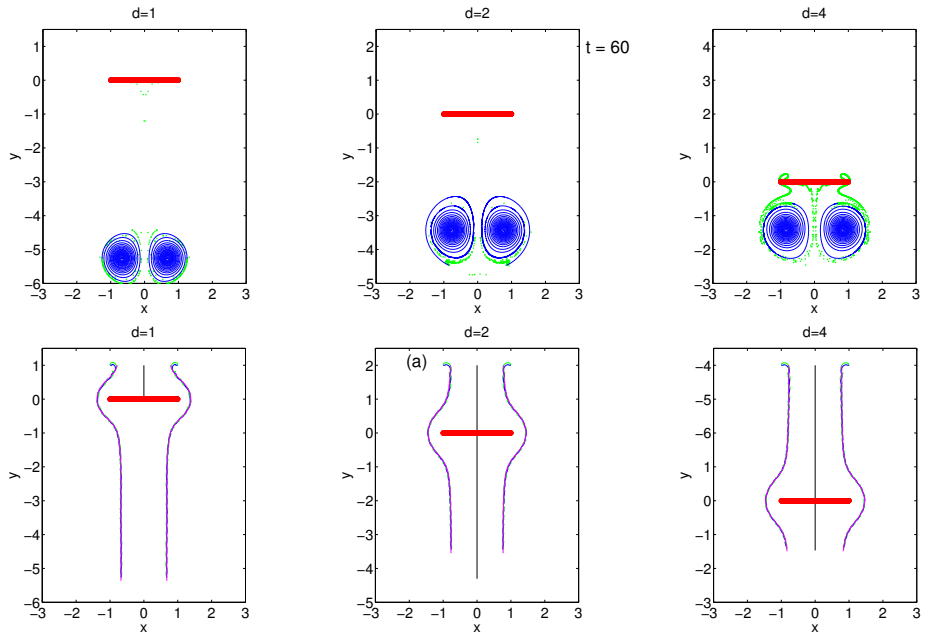


Figure 8: Solution for $d = 1, 2, 4$, as indicated, where $d$ is the distance of plate from initial sheet position, for $\delta = 0.2, \phi = 0$. The position of the sheet at $t = 60$ (top) and and the vortex core trajectories (bottom) are shown.

be observed near the spiral center. The position of the center depends somewhat on $\delta$. While the x-coordinate $x_c$ of the center remains almost unchanged as $\delta$ decreases, the y-coordinate $y_c$ at the final time is slightly more negative for smaller $\delta$. For example, for $\delta = 0.1$, $y_c \approx -3.5$, while for $\delta = 0.4$, $y_c \approx -3.2$.

The left column in figure 7 clearly shows the behaviour characteristic of the vortex sheet roll-up near the center. The spiral ends in the form of a small hook, formed by a change in concavity of the roll-up close to the end of the sheet. The resulting inflection point is the point $\boldsymbol{x}_I$ referred to in figures 6 and in the discussion of the point insertion method, in §4.3.

The right column in figure 7 shows the trajectory of the vortex center, approximated by the vortex sheet endpoints and the inflection point, as well as the middle point on the sheet with $\alpha = \pi/2$, and the two-point vortex approximation. A close inspection of this figure shows that as $\delta$ decreases, the vortex center oscillates with a smaller amplitude and higher frequency. Again, the spiral center is well approximated by the two-point-vortex approximation. The midpoint veers to the left of the straight downward trajectory for the smallest value of $\delta$. This is most likely caused by loss in resolution.

### 5.3. *Dependence on d*

Next, we vary the distance $d$ between the plate and the initial vortex sheet. Figure 8 plots the solution computed with $d = 1, 2, 4$, with $\delta = 0.2, \phi = 0$. The top row shows the vortex sheet position at the last time computed, $t = 60$. The bottom row shows the sprial center trajectory.

The top row shows that at $t = 60$ with $d = 4$, the vortex sheet has just moved past the plate. Comparison of the sheet position at $t = 60$ clearly shows that as $d$ increases, the vortex sheet travels less far. That is, the plate slows the sheet down, more so the

further it is from its initial position. This is also evident from the trajectories shown in the bottom row. As $d$ increases, the total distance travelled by the spiral centers, as well as by the two-point approximation, is smaller. It is interesting to note that with the smallest value of $d$ shown, $d = 1$, the total distance travelled is actually larger than in the absence of a plate, shown in figure 5, left column. That is, if the plate is close to the initial sheet, in speeds up the sheet's downward motion. As the plate is moved away from the initial sheet, it slows the motion down.

### 5.4. *Dependence on* $\phi$

Figure 9 shows the results if the plate is inclined away from the horizontal by an angle $\phi$, where we consider $\phi = \pi/12, \pi/6, \pi/4, \pi/3$, with $\delta = 0.2$, $d = 2$. The sheet position at $t = 60$ is shown at the left, the center trajectories (blue, green) and the two-point-vortex approximation (red) is shown at the right. The top row shows the smallest inclination angle, $\phi = \pi/12$. This case is thus closest to the case $\phi = 0$ considered previously. Remember that for $\phi = 0$, the vortices approached the plate at an angle normal to the plate and leave the plate on its other side also at an angle normal to it. For $\phi = \pi/12$ the situation is similar. The vortices approach the plate at an angle close to normal. After encountering the plate they leave the plate practically normal to it. Thus the plate deflects the trajectory by $\pi/12$.

As $\phi$ increases, the situation dramatically changes. In the top middle row, with $\phi = \pi/6$, the vortices leave the plate not normal to it, but close to parallel to it. Thus, for this value of $\phi$, the plate deflects the vortices in the opposite direction!

With the second largest angle, $\phi = \pi/4$, shown in the bottom middle row, this behaviour is even more evident: after the vortices encounter the plate, they leave the plate parallel to it, instead of normal to it.

For the largest angle $\phi = \pi/3$, shown in the bottom row, the vortices first run parallel to the plate while the plate is between them. Then they veer away in a straight line at an even further angle from horizontal.

Thus, encountering a plate at an angle deflects the trajectory of the vortices. If the plate is inclined little from the horizontal, the trajectory is deflected little from the vertical, and remains close to normal to the plate. If the plate in inclined far from the horizontal, the vortex is deflected in the opposite direction and leaves the plate almost parallel to it, instead of normal to it.

The observed behaviour is qualitatively similar in the two-point vortex approximation. However, for large angles $\phi$, the two-point vortex approximation is deflected further than the vortex sheet.

## 6. Summary

The evolution of an elliptically loaded vortex sheet in the presence of a plate in its path, of the same size as the sheet, is computed using a vortex method. The sheet rolls up into a spiral at each of its edges, forming a vortex pair that travels in a linear trajectory towards the plate. The two vortices then move around the plate and continue to follow a linear trajectory as they leave on the other side of the plate. When the vortex sheet hits the plate the sheet develops regions of high curvature and becomes difficult to resolve in those areas.

The vortex sheet motion is regularized numerically by introducing a parameter $\delta$ into the governing equations. We studied the dependence of the solution on the parameter $\delta$, on the distance $d$ of the plate from the initial sheet position, and on the inclination angle $\phi$ of the plate, relative to the oncoming vortex sheet trajectory.

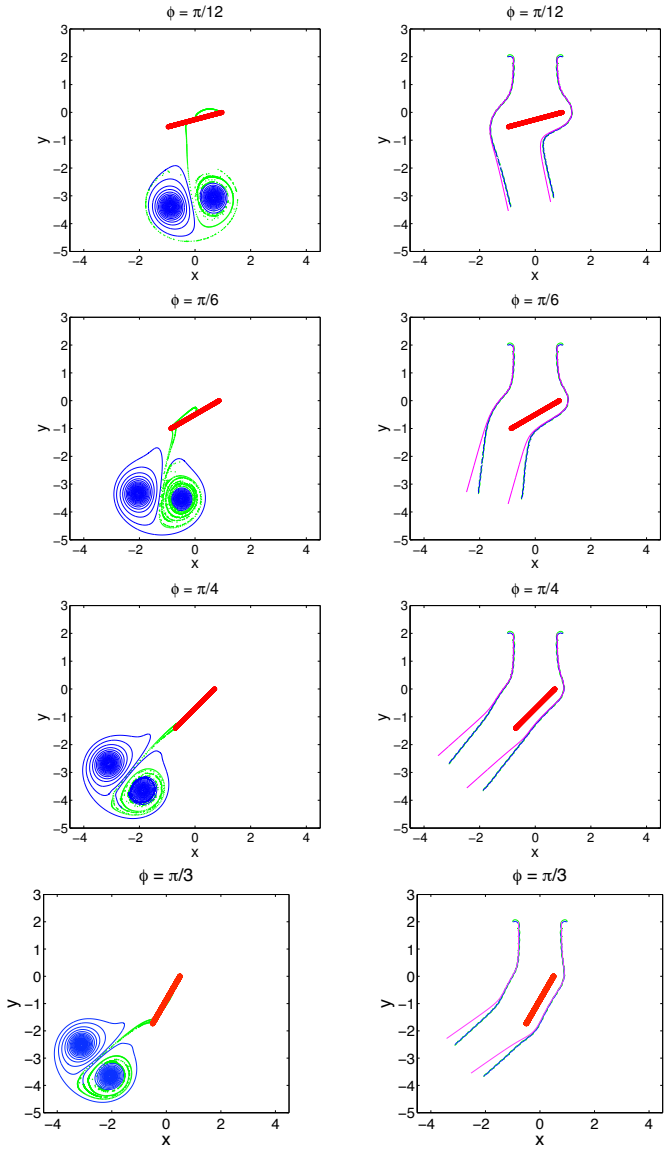


Figure 9: Solution for $\phi = \pi/12, \pi/6, \pi/4, \pi/3$, as indicated, for $d = 2, \delta = 0.2$. The position of the sheet at $t = 60$ (top) and the trajectories of the vortex core (blue/green) as well as the point vortex pair approximation (pink) are shown.

The following trends are observed.

• As $\delta$ decreases, the vortex sheet develops more spiral turns, forming a more tightly wound spiral. The vortex pair also travels slightly faster for smaller $\delta$.

• As we increase the distance $d$ of the plate from the initial sheet, the vortex sheet meets the plate at correspondingly later times. For small values of $d$, the sheet speeds up and travels faster than in the absence of any plate. As $d$ increases, the total distance travelled decreases slightly. Besides these effects, the vortex sheet trajectory is largely unaffected by $d$.

• The above results are obtained with the plate normal to the oncoming vortex sheet

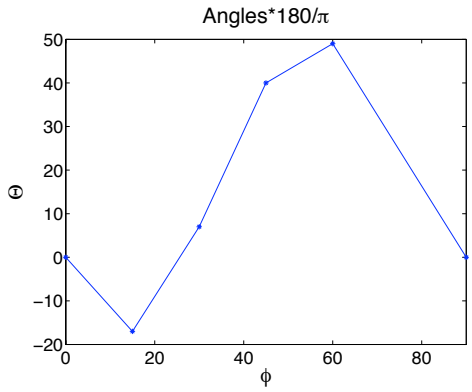


Figure 10: Graphical comparison of angles $\phi$ and $\Theta$, as indicated, for $d = 2, \delta = 0.2$ Values of $\Theta$ are measured clockwise from horizontally downward.

trajectory, corresponding to inclination angle $\phi = 0$. The inclination angle affects the direction of propagation of the vortex pair after it encounters the plate. For small values of $\phi$, the vortex pair leaves the plate normal to it, in the direction of inclination of the plate, and thus slightly displaced from the oncoming direction. However, for large values of $\phi$, the vortex pair leaves the plate almost parallel to the plate, in direction opposite of the direction of inclination of the plate. Therefore there seems to be a bifurcation in the direction of travel of the vortices as a function of $\phi$. We estimate this bifurcation by taking a cursory examination of the vortex deflection angle $\Theta$. Figure 10 shows that for $\phi = 0$ and $\phi = \pi$, $\Theta = 0$; we know this beforehand. For small values of $\phi$, $\Theta$ is deflected weakly counterclockwise. For larger values of $\phi < \pi$, the angle $\Theta$ is deflected strongly clockwise.

We compared the vortex sheet trajectory with the trajectory of a two-point-vortex approximation of the sheet with equal initial circulation and centroid in each half of the symmetry plane. We found that in all cases the two-point-vortex motion and the vortex sheet center trajectory were in very close agreement, with small angular discrepancies for $\phi > 0$.

## 7. Acknowledgements

I thank Professor Monika Nitsche for her guidance in this research. I also thank Professor Robert Krasny for suggesting the problem studied, and Dr. Robert Niemeyer for comments on the manuscript. Finally, I thank the National Science Foundation for supporting this research through the NSF-MCTP program, Mentoring through Critical Transition Points, at the University of New Mexico, via the NSF Award # DMS-1148801.

## REFERENCES

C. R. Anderson, 1986 A method of local corrections for computing the velocity field due to a distribution of vortex blobs. *J. Comput. Phys.*, **62**, 111–123.

G. R. Baker, 1979 The "Cloud in Cell" technique applied to the roll up of vortex sheets. *J. Comput. Phys.*, **31**, 76–95.

G. R. Baker, 1980 A test of the method of Fink & Soh for following vortex sheet motion. *J. Fluid Mech*, **10**, 209–220.

R. E. Caflisch, N. Ercolani, T. Y. Hou, & Y. Landis, 1993 Multi-valued solutions and

branch point singularities for nonlinear hyperbolic or elliptic systems. *Communications on pure and applied mathematics*, **46(4)**, 453–499.

A. J. Chorin & P. S. Bernard, 1973 Discretization of a vortex sheet, with an example of roll-up. *J. Comput. Phys.*, **13**, 423–429.

A. J. Chorin & J. E. A. Marsden, 1979 A Mathematical Introduction to Fluid Mechanics. *New York: Springer-Verlag.*

P. T. Fink & W. K. Soh, 1978 A new approach to roll-up calculations of vortex sheets. *Proc. R. Soc. Lond. A*, **362**, 195–209.

J. J. L. Higdon & C. Pozrikidis, 1985 The self-induced motion of vortex sheets. *J. Fluid Mech*, **150**, 203–231.

R. Krasny, 1986 A study of singularity formation in a vortex sheet by the point-vortex approximation. *J. Fluid Mech*, **167**, 65–93.

R. Krasny, 1986 Desingularization of periodic vortex sheet roll-up. *J. Comput. Phys.*, **65**, 292–313.

R. Krasny, 1987 Computation of vortex sheet roll-up in the Trefftz plane. *J. Fluid Mech*, **184**, 123–155.

A. Leonard, 1980 Review: vortex methods for flow simulation. *J. Comput. Phys.*, **37**, 289–335.

D. W. Moore, 1979 The spontaneous appearance of a singularity in the shape of an evolving vortex sheet. *Proc. R. Soc. Lond. A*, **365**, 105–119.

N. I. Muskhelishvili, 1953 Singular integral equations, boundary problems of function theory and their application to mathematical physics. Translated by J. R. M. Radok. *P. Noordhoff N. V. Groningen, Holland, reprinted by Dover in 1992.*

M. Nitsche, R. Krasny, 1994 A numerical study of vortex ring formation at the edge of a circular tube. *J. Fluid Mech*, **276**, 139–161.

S. C. Rennich & S. K. Lele, 1999 Method for accelerating the destruction of aircraft wake vortices. *J. Aircraft*, **36** (2), 398–404.

P. G. Saffman & G. R. Baker, 1979 Vortex interactions. *Ann. Rev. Fluid Mech.*, **11**, 95–121.

T. Sarpkaya, 1989 Computational methods with vortices – the 1988 Freeman Scholar Lecture. *J. Fluids Eng.*, **111**, 5–52.

M. J. Shelley, 1992 A study of singularity formation in vortex-sheet motion by a spectrally accurate vortex method. *J. Fluid Mech*, **244**, 493–526.

J. X. Sheng, A. Ysasi, D. Kolomenskiy, E. Kanso, M. Nitsche, & K. Schneider, K., 2012 Simulating vortex wakes of flapping plates. *IMA Volume on Natural Locomotion in Fluids and on Surfaces: Swimming, Flying, and Sliding.*

P. R. Spalart, 1998 Airplane trailing vortices. *Ann. Rev. Fluid Mech.*, **30**, 107–138.

G. Tryggvason, W. J. A. Dahm & K. Sbeih, 1991 Fine structure of vortex sheet rollup by viscous and inviscid simulation. *J. Fluids Eng.*, **113**, 31–36.